Geophysical Research Letters

RESEARCH LETTER
10.1029/2021GL094140

Hydroxyl Radical (OH) Response to Meteorological Forcing and Implication for the Methane Budget

Jian He[1,2,3], Vaishali Naik[2], and Larry Wayne Horowitz[2]

[1]Program in Atmospheric and Oceanic Sciences, Princeton University, Princeton, NJ, USA, [2]NOAA Geophysical Fluid Dynamics Laboratory, Princeton, NJ, USA, [3]Now at NOAA Chemical Sciences Laboratory/Cooperative Institute for Research in Environmental Sciences, University of Colorado, Boulder, CO, USA

Key Points:

- Hydroxyl radical (OH) abundances vary by up to 2% globally and by larger amounts regionally (>10%) when nudged with different meteorological reanalyses
- Meteorology-driven differences in OH lead to differences of 11.2 Tg yr^{-1} in estimated methane emissions and 0.24 years in methane lifetime
- Meteorology affects OH concentrations but not the OH trend, with the latter showing strong correlation with reactive nitrogen emissions

Supporting Information:

Supporting Information may be found in the online version of this article.

Correspondence to:

J. He,
jianhe.phd@gmail.com

Citation:

He, J., Naik, V., & Horowitz, L. W. (2021). Hydroxyl radical (OH) response to meteorological forcing and implication for the methane budget. *Geophysical Research Letters*, *48*, e2021GL094140. https://doi.org/10.1029/2021GL094140

Received 4 MAY 2021
Accepted 3 AUG 2021

Abstract The hydroxyl radical (OH) is a powerful oxidant in the troposphere controlling the atmospheric lifetimes of many short-lived climate forcers such as methane. In this study, the GFDL-AM4.1 model is used to investigate the meteorological impacts on OH and the methane budget and lifetime over 1980–2017. Driven by meteorological reanalyses from the National Centers for Environmental Prediction and the Modern-Era Retrospective analysis for Research and Applications (Version 2), our model gives an 11.2 Tg yr^{-1} difference in the derived methane emissions and 0.24 years difference in the estimated methane lifetime. The results suggest that meteorology affects the mean OH concentrations but not OH trend, while the latter shows strong correlation with reactive nitrogen emissions. Despite the relatively small difference in global tropospheric OH (~2%) induced by different meteorological forcings, the difference is much larger regionally, leading to a difference of 8 Tg yr^{-1} in tropical methane emissions.

Plain Language Summary The hydroxyl radical (OH) is extremely reactive in the atmosphere and able to destroy many other chemicals, such as methane, a strong greenhouse gas that contributes significantly to global warming. Therefore, OH is very important for methane concentrations and lifetime. Changes in the meteorological features (e.g., temperature, wind patterns, and relative humidity) would affect OH in the atmosphere. In this study, we use a three-dimensional numerical model to understand the meteorological impacts on OH and the resulting impacts on methane budget and lifetime over 1980–2017. With different meteorological datasets, we find there is a 2% difference in global mean tropospheric OH concentrations, with much larger differences over tropics. We calculate methane sources and loss due to OH and find an 11.2 Tg yr^{-1} difference in the global mean methane sources with 8 Tg yr^{-1} difference in the tropics, and 0.24 years difference in methane lifetime between the two meteorological datasets.

1. Introduction

The hydroxyl radical (OH) is a powerful oxidizing agent in the troposphere controlling the atmospheric lifetimes of many short-lived climate forcers (SLCFs). For example, methane (CH_4), a well-mixed greenhouse gas that is short-lived compared to carbon dioxide (CO_2), is removed from the atmosphere mainly through its reaction with OH in the troposphere, thereby influencing its budget and lifetime and therefore its climate impact. The global abundance and distribution of OH are primarily controlled by nonlinear atmospheric chemistry driven by emissions of SLCFs and modulated by meteorology. Here, we investigate the influence of uncertainty in OH induced by uncertainties in meteorology on the budget and lifetime of methane.

OH concentrations respond to a number of factors, namely: concentrations of ozone (O_3); emissions of nitrogen oxide (NO_x), carbon monoxide (CO), and volatile organic compounds (VOCs); and meteorology, namely temperature, water vapor, and ultraviolet radiation (Spivakovsky et al., 2000). Intercomparison of results from global atmospheric chemistry models show significant intermodel diversity in the simulated OH distribution, variability, and trends (Naik, Voulgarakis, et al., 2013; Voulgarakis et al., 2013; Zhao et al., 2019). This model diversity has been primarily attributed to differences in chemical mechanisms that result in differences in the chemical drivers of OH (Nicely et al., 2020; Wild et al., 2020; Zhao et al., 2019). An additional possible source of diversity is differences in meteorology across models that arise either because models produce their own meteorology (free-running) (e.g., Stevenson et al., 2020; Zhao et al., 2019) or are forced by reanalyzed meteorological fields (nudged) (e.g., Dalsøren et al., 2016). Differences in the

representations of dynamics and transport in the free-running models and different nudging approach for large-scale flows and different reanalysis products in nudged models could lead to differences in modeled meteorology (Orbe et al., 2020). These differences lead to different large-scale dynamical features, such as the El Niño-Southern Oscillation (ENSO), which play an important role in regulating OH variability (Anderson et al., 2021; Turner et al., 2017).

To estimate the global and regional methane budget, atmospheric observations are combined with chemical transport models (CTMs) either with interactive OH chemistry or prescribed OH fields. In the bottom-up process-based model approach, the methane-OH sink is explicitly simulated in the model with consideration of methane-OH feedback (e.g., Dalsøren et al., 2016; He et al., 2020); however, model-to-model differences in OH, as noted above, introduce uncertainty in methane budget and lifetime. In the top-down inverse modeling approach, methane emissions are optimized by assimilating observations while OH concentrations are prescribed (either based on the climatological OH fields from model output or inferred from observations) (e.g., Patra et al., 2016; Rice et al., 2016; Tsuruta et al., 2017) and uncertainties in the estimated global and regional methane budget are solely attributed to methane emissions (Saunois et al., 2020). In a recent study, Zhao et al. (2020) evaluated the influence of spatio-temporal variations in OH on the top-down estimate of global and regional methane budget by implementing OH fields from 10 chemistry models participating in the Chemistry-Climate Model Imitative (CCMI) in a four-dimensional inversion system. They found that the uncertainties in the derived methane emissions were similar to those estimated from bottom-up approaches and greater than those reported for top-down estimates, highlighting the need for better quantification of uncertainties in OH distribution and spatio-temporal variability.

In this study, we explore uncertainties in OH distribution, trends, and variability, and the resulting impacts on the methane budget and lifetime due to differences in meteorology. We apply simulations of the full-chemistry version of the Geophysical Fluid Dynamics Laboratory (GFDL) new-generation Atmospheric Model, version 4.1 (AM4.1; Horowitz et al., 2020; Zhao et al., 2018a, 2018b) nudged to two different reanalysis products to investigate meteorology-driven uncertainties in OH.

2. Model Description and Simulation Design

We use GFDL-AM4.1, the atmospheric component of the new generation GFDL Earth System Model (ESM4) (Dunne et al., 2020). The physics and dynamics of AM4.1 are built upon GFDL's AM4.0 atmospheric model (Zhao et al., 2018a, 2018b) and include fully interactive tropospheric and stratospheric chemistry described in detail by Horowitz et al. (2020). In its standard form, the model setup consists of a cubed sphere finite-volume dynamical core with a horizontal resolution of ~100 km and 49 vertical levels extending from the surface up to ~80 km. The model's lowermost level is ~30 m thick. The chemical scheme includes a total of 58 prognostic gas-phase tracers, 18 prognostic aerosol tracers, 5 prognostic ideal tracers, and 40 diagnostic chemical tracers, with 43 photolysis reactions (with photolysis rates calculated based on Fast-JX (Li et al., 2016) and dependent on simulated ozone, aerosols, and clouds), 190 gas-phase kinetic reactions, and 15 heterogeneous reactions in this version of AM4.1 to represent tropospheric and stratospheric chemistry.

We conduct several hindcast simulations for 1980–2017, as listed in Table S1, to investigate the OH response to different meteorological forcing. We start with a standard model configuration, following Atmospheric Model Intercomparison Project (AMIP) protocol, which forces the model with prescribed interannually varying sea surface temperatures and sea ice (Taylor et al., 2000) without atmospheric nudging. This experiment is referred to as "AMIP." The sensitivity experiments with horizontal winds nudged to the National Centers for Environmental Prediction (NCEP) reanalysis (Kalnay et al., 1996) and the Modern-Era Retrospective analysis for Research and Applications, Version 2 (MERRA-2) (Gelaro et al., 2017) are referred to as "NCEP" and "MERRA", respectively. In both NCEP and MERRA experiments, we use a pressure-dependent nudging technique (Lin et al., 2012) and apply a relaxation time scale of 6 h to the nudged fields. In these three experiments, methane concentrations are prescribed as lower boundary conditions, which is a standard AMIP configuration. We also conduct two additional methane emission-driven experiments, forced by NCEP and MERRA-2 reanalysis and referred to as "NCEPe" and "MERRAe," to take a closer look at the regional impacts. We constrain methane emissions with surface methane observations from the Global Monitoring Laboratory (GML) of the National Oceanic and Atmospheric Administration (NOAA), as described

in He et al. (2020), for these two experiments. Since OH concentrations are different due to different meteorology, the optimized methane emissions are therefore different in NCEPe and MERRAe. For all the nudged experiments, only horizontal winds are nudged to the reanalysis to allow all other meteorological fields to evolve under the model physics and avoid possible unintentional perturbation on the model states.

Anthropogenic and biomass burning emissions of short-lived species are same as those in He et al. (2020), compiled from the Community Emissions Data System (CEDS, version May 18, 2017, Hoesly et al., 2018) and van Marle et al. (2017) for 1980–2014, and from a middle-of-the-road scenario of Shared Socioeconomic Pathways targeting a forcing level of 4.5 W m^{-2} (SSP2-4.5; Gidden et al., 2019) for 2015–2017. Natural emissions of short-lived species are from Naik, Horowitz, et al. (2013). The online emission calculations including biogenic VOCs, dimethyl sulfide (DMS), lightning NO_x (LNO_x), dust, and sea salt are described in Text S1. These emissions depend on the simulated meteorology in the model and thus are different among the three simulations as summarized in Table S2.

3. Results and Discussions

3.1. Comparisons of OH and Major Drivers

Figure 1 shows the comparisons of zonal mean OH concentrations and its major drivers (temperature, specific humidity, lighting NO_x emissions, and ozone photolysis rate) from AMIP, NCEP, and MERRA simulations. The climatological mean of tropospheric mean fields is summarized in Table S3. Compared to NCEP, MERRA generally simulates slightly higher temperature in most regions, but lower temperature in the upper troposphere at high latitudes. Significant differences exist in tropospheric specific humidity (Q). For example, MERRA simulates much higher Q in the low latitudes of the Northern Hemisphere (by up to 20%), whereas lower Q in the low latitudes over Southern Hemisphere (by up to 10%). These differences in Q are consistent with those in LNO_x (e.g., >10% in middle and higher troposphere over the tropics), which could be due in part to the differences in convection in the two simulations. The differences in wind reanalysis between MERRA and NCEP induce different ocean evaporation and mixing, leading to different humidity and deep convection. Compared to AMIP, both NCEP and MERRA simulate higher ozone photolysis rate (J_{O_3}) over tropics but lower ozone photolysis rate over middle and higher latitudes due to different clouds simulated in the model. As a result, compared to AMIP and MERRA, NCEP simulates lower OH concentrations over low latitudes, especially in the lower troposphere. In the middle and upper troposphere, MERRA simulates much higher OH concentrations (by 4%–8%) than NCEP especially over the tropics, where strong solar radiation and convection occur.

Similar differences also exist in surface OH concentrations. Figure 2 shows the relative difference in surface OH and tropospheric OH (air-mass weighted) concentrations among the three simulations. Compared to AMIP simulation, both NCEP and MERRA simulate lower surface OH over the Northern Hemisphere and higher surface OH over the Southern Hemisphere. Compared to NCEP, MERRA generally simulates higher surface OH over most regions, except the areas along the Intertropical Convergence Zone and high latitudes in the Southern Hemisphere. Similarly, MERRA simulates higher tropospheric OH concentrations than NCEP over most of the globe. Despite the relatively small global mean differences in surface and tropospheric OH (i.e., 1.0% and 2.0%), much larger differences exist regionally. The largest difference occurs over the tropics, with >10% difference over tropical Africa, Southeast Asia, tropical Pacific Ocean, tropical South America, and Southern Cone. Those differences are associated with different dynamical and thermodynamic processes simulated in the model induced by different reanalyses.

Despite the nonlinearity of the chemical and dynamical system, several meteorological and chemical drivers are identified to have major controls on global mean tropospheric OH concentrations. Murray et al. (2014) found a linear relationship between global mean tropospheric OH concentrations and $J_{O_3} Q S_N \left(S_C^{-3/2}\right)$, where J_{O_3} represents tropospheric mean ozone photolysis rate, Q represents tropospheric mean specific humidity, S_N represents the tropospheric sources of reactive nitrogen, and S_C represents the tropospheric sources of reactive carbon. This linear relationship also exists in our simulations as shown in Figure S1. There is a strong linear dependence of global mean tropospheric OH concentrations on $J_{O_3} Q S_N \left(S_C^{-3/2}\right)$ in all three simulations, with $R^2 = 0.8$. Specifically, OH concentrations show strong linear dependence on

10.1029/2021GL094140

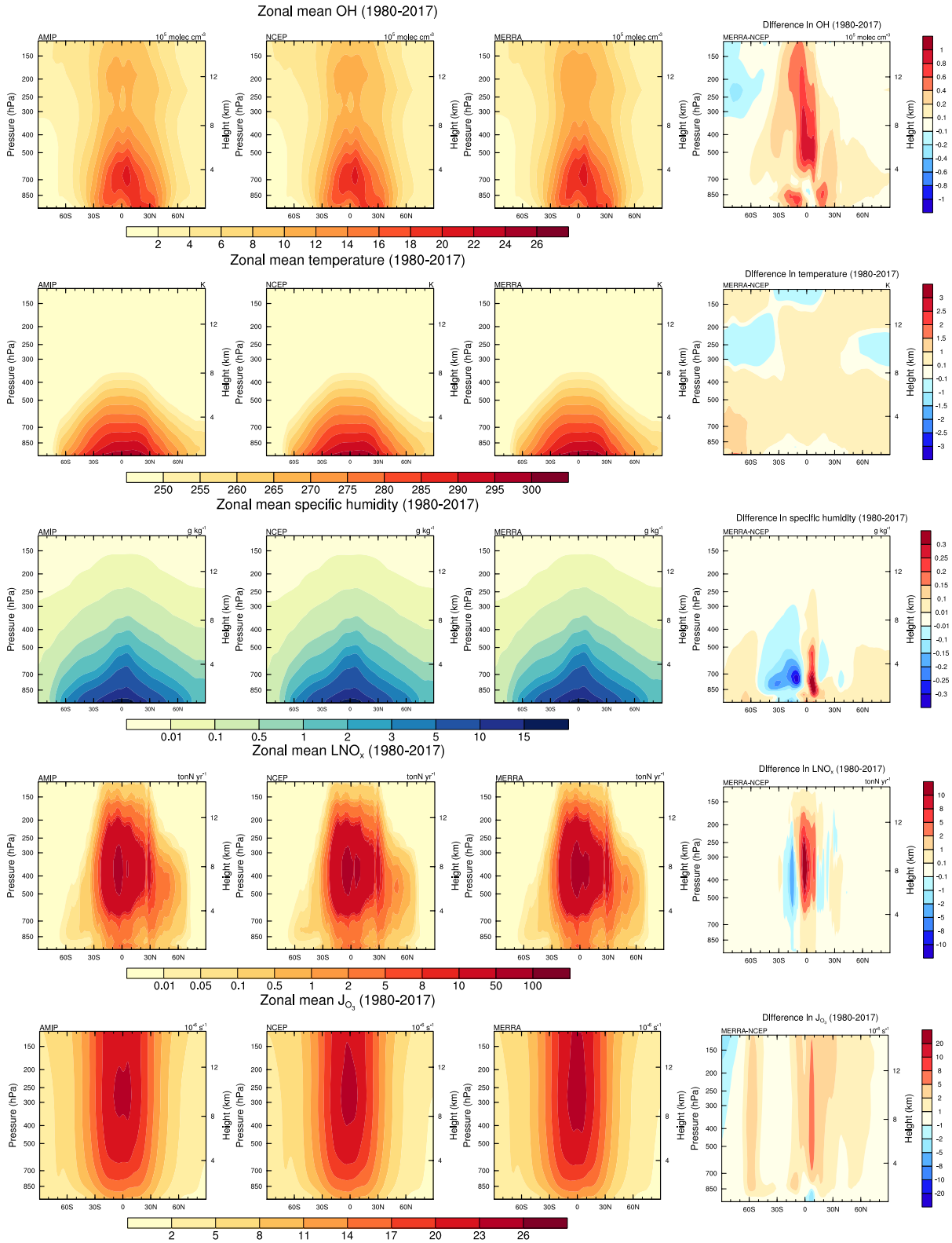

Figure 1.

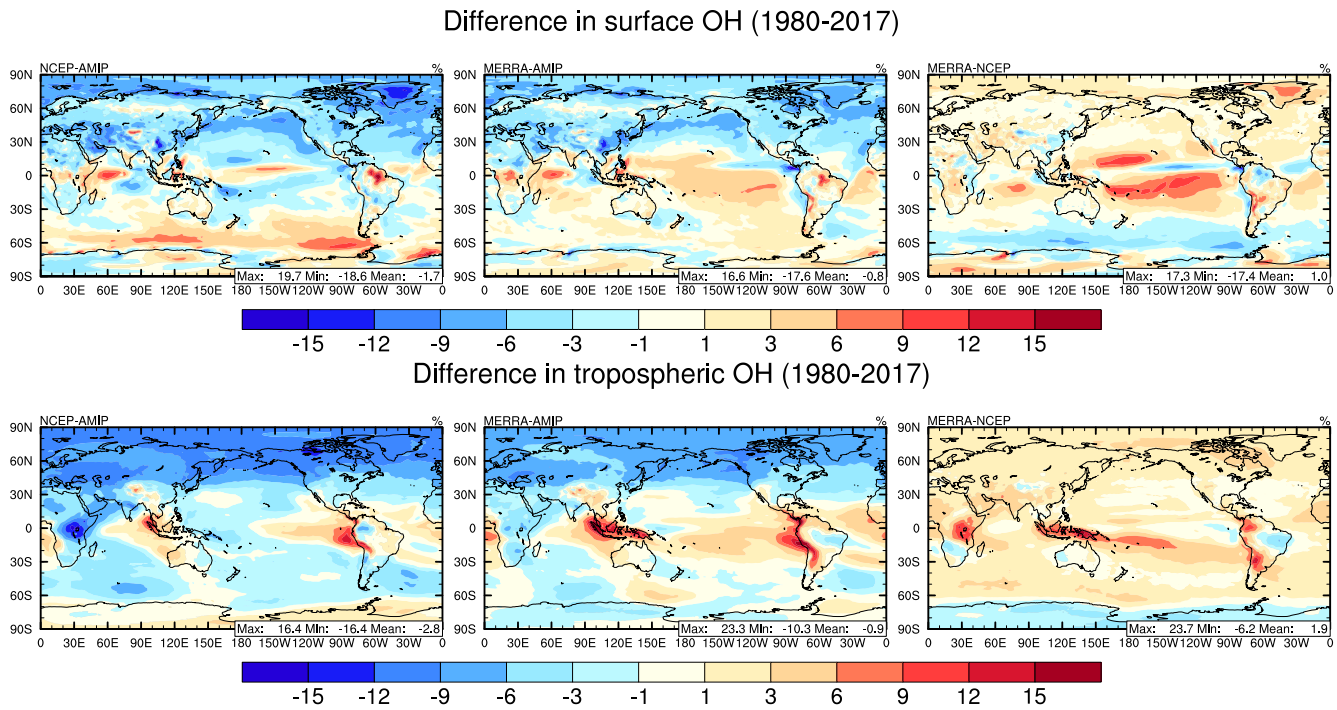

Figure 2. Relative difference (shown in percentage, %) in surface hydroxyl radical (OH) (row 1) and tropospheric air-mass weighted mean OH (row 2) concentrations among the simulation using Atmospheric Model Intercomparison Project (AMIP) protocol, and simulations driven by wind reanalysis from National Centers for Environmental Prediction (NCEP), and Modern-Era Retrospective analysis for Research and Applications, Version 2 (MERRA).

S_N (R^2 = 0.7–0.8) with weaker linear dependence on Q (R^2 = 0.4) and $S_C^{-3/2}$ (R^2 = 0.2) and no significant dependence on J_{O_3}. The strong linear dependence of OH concentrations on S_N suggests that interannual variability of global OH is highly correlated with NO_x emissions (mainly by LNO_x emissions), consistent with previous studies (e.g., Fiore et al., 2006; Murray et al., 2013).

Figure 3 shows the time series of tropospheric OH concentrations, tropical CO emissions, global mean methane emissions, tropical total NO_x emissions, tropical NO_x emissions without LNO_x, and global mean LNO_x emissions over 1980–2017. Despite differences in mean tropospheric OH driven by the different meteorological forcing, all three simulations show an overall increasing trend in OH concentrations, which agrees well with those simulated by the CCMI models (e.g., Zhao et al., 2019). This suggests that meteorology could affect the magnitudes of mean OH concentrations, but not the trend. Similar findings are also shown in Gaubert et al. (2017), where they used the ensemble-based Data Assimilation Research Testbed (DART) (Anderson et al., 2009) and MERRA-2 meteorology. Stevenson et al. (2020) suggests the simulated increasing trend in OH concentrations is mainly due to the increases in tropical NO_x emissions, which is also shown in our study. As shown in Figure 3, despite the increases in CO and CH_4 emissions, the increases in tropical NO_x emissions dominate the increasing trend in OH. The increases in tropical NO_x emissions are mainly due to the increases in the prescribed tropical anthropogenic NO_x emissions and a slight increasing trend in LNO_x emissions simulated in the model, which remains to be tested by analysis of past observations. He et al. (2020) showed a −6% and +9% difference in global mean tropospheric OH concentrations when applying scaling factors of 0.5 and 2.0 to LNO_x emissions. Due to the strong correlations between OH concentrations and NO_x emissions, the impacts on OH due to different LNO_x emissions are much larger than those due to different meteorological forcing estimated in this study (i.e., ∼2%). This also suggests that

Figure 1. Zonal distribution of climatological mean (1980–2017) hydroxyl radical concentrations (OH, 10^5 molecules cm^{-3}, row 1), temperature (K, row 2), specific humidity (g kg^{-1}, row 3), lightning NO_x emissions (LNO_x, tonN yr^{-1}, row 4), and ozone photolysis rate (J_{O_3}, 10^{-6} s^{-1}, row 5) from the simulation using Atmospheric Model Intercomparison Project (AMIP) protocol, and simulations driven by wind reanalysis from National Centers for Environmental Prediction (NCEP) and Modern-Era Retrospective analysis for Research and Applications, Version 2 (MERRA), and the absolute difference between NCEP and MERRA (right column).

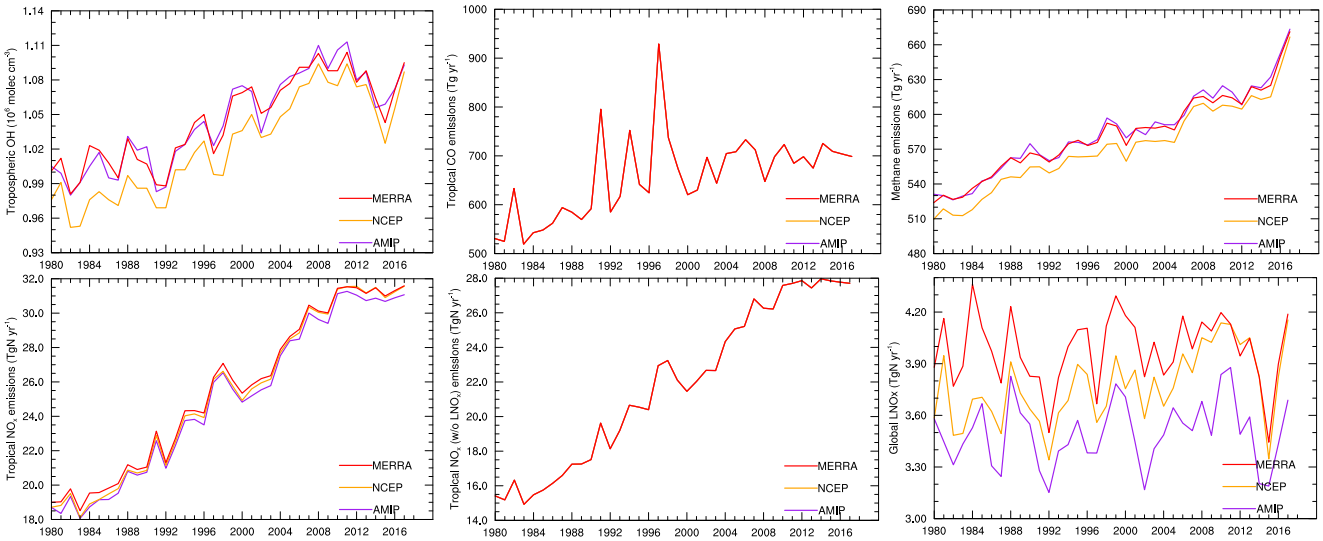

Figure 3. Global tropospheric air-mass weighted hydroxyl radical (OH) concentrations, tropical carbon monoxide (CO) emissions, global mean methane emissions, tropical nitrogen oxide (NO_x) emissions, tropical NO_x emissions without lightning NO_x (LNO_x), and global mean LNO_x emissions over 1980–2017.

better constraints on NO_x emissions (especially LNO_x) are necessary to reduce model uncertainty in OH estimates. On the other hand, the important role of LNO_x emissions on OH and methane lifetime is not only demonstrated in GFDL-AM4 model but also in other models. For example, Murray et al. (2013) found that the interannual variability in tropospheric OH is highly sensitive to LNO_x in GEOS-chem model. Wild et al. (2020) found LNO_x as the largest contributor to the methane lifetime in RSGC/UCI CTM and CAM-Chem and as the second largest contributor in GISS model.

3.2. Implications for Methane Budget

Different meteorological forcing leads to different OH levels, and therefore results in different estimates for methane emissions and lifetime. Table 1 summarizes the methane budget estimated from all the simulations. The methane emissions derived from concentration-driven simulations are based on mass balance, that is, the annual change of methane burden equals to the methane sources minus sinks. Since the differences in OH levels between MERRA and AMIP are small, the differences in derived methane emissions between MERRA and AMIP are also small, with an average of −1.8 Tg yr^{-1}. However, much larger differences exist in OH levels between MERRA and NCEP, leading to an average of +11.2 ± 3.5 Tg yr^{-1} difference in derived methane emissions. Specifically, during the methane stabilization period (i.e., 1999–2006), the difference in derived methane emissions between MERRA and NCEP varies from 8.5 to 15.0 Tg yr^{-1}, with an average of 11.9 Tg yr^{-1}. This magnitude of the difference is much larger than the imbalance (i.e., sources minus sinks) during this period, demonstrating the critical impacts of OH levels on methane emission estimates. On the other hand, OH differences are much larger regionally, especially over the tropics. For

Table 1
1980–2017 Methane Budget and Tropospheric Hydroxyl Radical (OH) (Annual Mean ± Standard Deviation)

	AMIP	NCEP	MERRA	NCEPe	MERRAe
Emissions (Tg yr^{-1})	584 ± 35	571 ± 37	583 ± 35	565 ± 35	576 ± 33
Sinks (Tg yr^{-1})	562 ± 42	549 ± 43	561 ± 41	545 ± 42	555 ± 40
Tropospheric lifetime (years)	10.0 ± 0.4	10.2 ± 0.5	10.0 ± 0.4	10.2 ± 0.5	9.9 ± 0.4
OH (10^6 molecules cm^{-3})[a]	1.05 ± 0.04	1.03 ± 0.04	1.04 ± 0.04	1.02 ± 0.04	1.05 ± 0.04

Abbreviations: AMIP, Atmospheric Model Intercomparison Project; MERRA, Modern-Era Retrospective analysis for Research and Applications, Version 2; NCEP, National Centers for Environmental Prediction.
[a]Rounded to two decimal places.

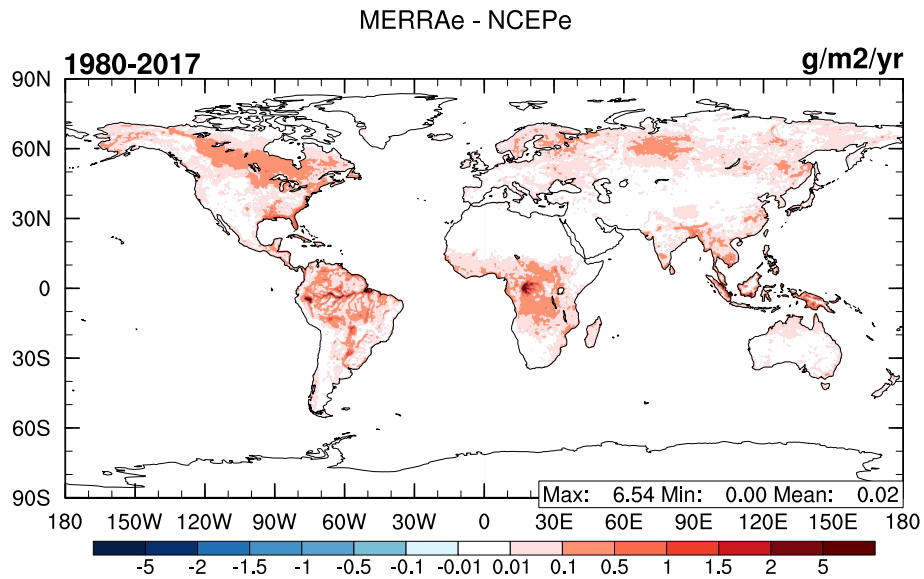

Figure 4. Absolute difference in methane emissions between MERRAe and NCEPe based on 1980–2017 annual mean.

example, OH difference between MERRA and NCEP varies from 3% to 6% over most of the tropical regions, with much larger differences over tropical Africa, Southeast Asia, tropical Pacific Ocean, tropical South America, and South Cone (>10%). Such differences can have significant impacts on estimated regional methane emissions. Previous studies suggest increases in tropical emissions are responsible for recent global methane growth (Lunt et al., 2019; Schaefer et al., 2016), while methane emissions over Southeast Asia are likely overestimated (Patra et al., 2016). With such large differences in OH levels over the tropics, it is a great challenge to build confidence in derived methane emissions from inverse modeling with prescribed OH fields.

As methane burdens are very similar in the three simulations (due to prescribed lower boundaries), with different OH concentrations in AMIP, NCEP, and MERRA experiments, the tropospheric methane lifetimes are slightly different, with NCEP having a 0.28 years longer methane lifetime than AMIP and MERRA having a similar methane lifetime as AMIP.

Emissions derived from concentration-driven simulations such as the above only represent global totals and do not have regional features. To investigate regional impacts, we further scrutinize the emission-driven simulations. Figure 4 shows the absolute difference in the optimized methane emissions between NCEPe and MERRAe. Time series of methane budget can be found in Figure S2. Methane emissions in MERRAe are in general higher than those in NCEPe. The differences in optimized methane emissions in the two emission-driven simulations are about +11.0 ± 4.5 Tg yr^{-1} during 1980–2017 (with +11.7 Tg yr^{-1} during 1999–2006 and +7.0 Tg yr^{-1} during 2007–2017). In the emission-driven simulations, we produce similar simulated methane concentrations by constraining methane emissions with surface methane observations. Therefore, the emissions derived for the MERRAe simulation are higher to offset the impacts from the higher simulated OH concentrations with MERRA. The differences in OH concentrations between NCEPe and MERRAe range from 0.4% to 4.9%, with a global average of 2.2% and the tropical average of 2.4%. As a result, methane emissions derived for MERRAe are about 5%–54% higher than NCEPe over most of the tropical region, which is about 8 Tg yr^{-1} higher over 30°S–30°N, and 3 Tg yr^{-1} (<5%) higher mainly over 30°–90°N (see Figure 4). With similar methane burdens but different OH concentrations in the NCEPe and MERRAe experiments, the tropospheric methane lifetimes range from 9.9 to 10.2 years with a difference of 0.24 years.

The annual mean estimated emissions from emission-driven simulations are about 7 Tg yr^{-1} lower than those from concentration-driven simulations. The prescribed methane concentrations are derived by Meinshausen et al. (2017) to be used in the Climate Model Intercomparison Project-Phase 6 (CMIP6) experiments, which considers both polluted events and background conditions. The surface observations used for the methane emission optimization is solely based on NOAA GML flask measurements from remote sites

as described in He et al. (2020). Therefore, the prescribed methane concentrations are slightly higher than those from NOAA GML measurements. Despite similar annual changes in the methane burden, methane loss is larger in concentration-driven simulations than emission-driven simulations, leading to higher derived methane emissions (see Table 1). However, the differences in the derived methane emissions and tropospheric methane lifetime due to different meteorological forcing are similar in the emission-driven and concentration-driven simulations. Globally, a 1% difference in OH levels could lead to about 5 Tg yr^{-1} difference in estimated methane emissions, which is comparable to previous estimates (He et al., 2020).

4. Summary

In this study, GFDL-AM4.1 model simulations are conducted to investigate the OH response to different meteorological forcing. Climatological global mean tropospheric OH concentrations differ across the three simulations, with the AMIP simulation producing the highest while the NCEP simulation produces the smallest level. Forced by the MERRA-2 reanalysis, the model estimates higher tropospheric OH concentrations than that forced by the NCEP reanalysis (by ~2%), with >10% higher OH concentrations over tropics (e.g., tropical Africa, Southeast Asia, tropical Pacific Ocean, tropical South America, and South Cone). There is an overall increasing trend in tropospheric OH concentrations in all the model simulations (with or without atmospheric nudging). Results also suggest a strong linear dependence of OH concentrations on reactive nitrogen emissions. The model simulation driven by the MERRA-2 reanalysis suggests derived methane emissions (based on mass balance) are higher than those using the NCEP reanalysis by 11.2 Tg yr^{-1} and a lower estimated tropospheric methane lifetime by 0.24 years.

The model simulations driven by methane emissions forced with different meteorological reanalyses further confirm the significant impacts of OH on derived methane emissions. Constrained with surface methane observations, methane emissions are optimized to force the model to reproduce observed methane trends and variability. Forced by different meteorological reanalyses, the model estimates different OH concentrations (by ~2%), leading to 11.0 Tg yr^{-1} and 0.24 years difference in the estimated optimized methane emissions and methane lifetime, similar to those from the concentration-driven simulations.

The results also suggest that meteorology affects the mean OH concentrations but not OH trend, while the latter shows strong correlation with reactive nitrogen emissions (mainly tropical NO_x emissions). Despite the relatively small difference in global mean tropospheric OH concentrations due to different meteorological forcing (~2%), the difference in OH concentrations are much larger regionally and therefore the difference in the derived methane emissions can be significant (e.g., 8 Tg yr^{-1} over tropics estimated in this study). This demonstrates the critical role of OH in estimating the methane budget, no matter whether a top-down inversion or bottom-up approach is used, highlighting the need to better constrain OH abundances and variations.

Data Availability Statement

Methane surface observations are downloaded from the NOAA Global Monitoring Laboratory (www.esrl.noaa.gov/gmd/ccgg/trends_ch4/). NCEP data are downloaded from the NCAR Research Data Archive (https://rda.ucar.edu/datasets/ds090.0/) and MERRA2 data are downloaded from https://search.earthdata.nasa.gov/search?q=M2T3NVASM.

Acknowledgments
This work is supported by the Carbon Mitigation Initiative at Princeton University. The authors also thank the GFDL model development team for developing the ESM4.1/AM4.1.

References

Anderson, D. C., Duncan, B. N., Fiore, A. M., Baublitz, C. B., Follette-Cook, M. B., Nicely, J. M., & Wolfe, G. M. (2021). Spatial and temporal variability in the hydroxyl (OH) radical: Understanding the role of large-scale climate features and their influence on OH through its dynamical and photochemical drivers. *Atmospheric Chemistry and Physics*, *21*, 6481–6508. https://doi.org/10.5194/acp-21-6481-2021

Anderson, J., Hoar, T., Raeder, K., Liu, H., Collins, N., Torn, R., & Avellano, A. (2009). The data assimilation research testbed: A community facility. *Bulletin of the American Meteorological Society*, *90*, 1283–1296. https://doi.org/10.1175/2009bams2618.1

Dalsøren, S. B., Myhre, C. L., Myhre, G., Gomez-Pelaez, A. J., Søvde, O. A., Isaksen, I. S. A., et al. (2016). Atmospheric methane evolution the last 40 years. *Atmospheric Chemistry and Physics*, *16*, 3099–3126. https://doi.org/10.5194/acp16-3099-2016

Dunne, J. P., Horowitz, L. W., Adcroft, A. J., Ginoux, P., Held, I. M., John, J. G., et al. (2020). The GFDL Earth system model version 4.1 (GFDL-ESM4.1): Overall coupled model description and simulation characteristics. *Journal of Advances in Modeling Earth Systems*, *12*, e2019MS002015. https://doi.org/10.1029/2019MS002015

Fiore, A. M., Horowitz, L. W., Dlugokencky, E. J., & West, J. J. (2006). Impact of meteorology and emissions on methane trends, 1990–2004. *Geophysical Research Letters*, *33*, L12809. https://doi.org/10.1029/2006GL026199

Gaubert, B., Worden, H. M., Arellano, A. F. J., Emmons, L. K., Tilmes, S., Barré, J., et al. (2017). Chemical feedback from decreasing carbon monoxide emissions. *Geophysical Research Letters*, *44*, 9985–9995. https://doi.org/10.1002/2017gl074987

Gelaro, R., McCarty, W., Suárez, M. J., Todling, R., Molod, A., Takacs, L., et al. (2017). The modern-era retrospective analysis for research and applications, version 2 (MERRA-2). *Journal of Climate*, *30*, 5419–5454. https://doi.org/10.1175/jcli-d-16-0758.1

Gidden, M. J., Riahi, K., Smith, S. J., Fujimori, S., Luderer, G., Kriegler, E., et al. (2019). Global emissions pathways under different socioeconomic scenarios for use in CMIP6: A dataset of harmonized emissions trajectories through the end of the century. *Geoscientific Model Development*, *12*, 1443–1475. https://doi.org/10.5194/gmd-12-1443-2019

He, J., Naik, V., Horowitz, L. W., Dlugokencky, E., & Thoning, K. (2020). Investigation of the global methane budget over 1980–2017 using GFDL-AM4.1. *Atmospheric Chemistry and Physics*, *20*, 805–827. https://doi.org/10.5194/acp-20-805-2020

Hoesly, R. M., Smith, S. J., Feng, L., Klimont, Z., Janssens-Maenhout, G., Pitkanen, T., et al. (2018). Historical (1750–2014) anthropogenic emissions of reactive gases and aerosols from the Community Emissions Data System (CEDS). *Geoscientific Model Development*, *11*, 369–408. https://doi.org/10.5194/gmd-11-369-2018

Horowitz, L. W., Naik, V., Paulot, F., Ginoux, P. A., Dunne, J. P., Mao, J., et al. (2020). The GFDL global atmospheric chemistry-climate model AM4.1: Model description and simulation characteristics. *Journal of Advances in Modeling Earth Systems*, *12*, e2019MS002032. https://doi.org/10.1029/2019MS002032

Kalnay, E., Kanamitsu, M., Kistler, R., Collins, W., Deaven, D., Gandin, L., et al. (1996). The NCEP/NCAR 40-year reanalysis project. *Bulletin of the American Meteorological Society*, *77*(3), 437–471. https://doi.org/10.1175/1520-0477(1996)077<0437:tnyrp>2.0.co;2

Li, J., Mao, J., Min, K.-E., Washenfelder, R. A., Brown, S. S., Kaiser, J., et al. (2016). Observational constraints on glyoxal production from isoprene oxidation and its contribution to organic aerosol over the Southeast United States. *Journal of Geophysical Research*, *121*, 9849–9861. https://doi.org/10.1002/2016JD025331

Lin, M., Fiore, A. M., Horowitz, L. W., Cooper, O. R., Naik, V., Holloway, J., et al. (2012). Transport of Asian ozone pollution into surface air over the western United States in spring. *Journal of Geophysical Research: Atmospheres*, *117*, D00V07. https://doi.org/10.1029/2011JD016961

Lunt, M. F., Palmer, P. I., Feng, L., Taylor, C. M., Boesch, H., & Parker, R. J. (2019). An increase in methane emissions from tropical Africa between 2010 and 2016 inferred from satellite data. *Atmospheric Chemistry and Physics*, *19*, 14721–14740. https://doi.org/10.5194/acp-19-14721-2019

Meinshausen, M., Vogel, E., Nauels, A., Lorbacher, K., Meinshausen, N., Etheridge, D. M., et al. (2017). Historical greenhouse gas concentrations for climate modelling (CMIP6). *Geoscientific Model Development*, *10*, 2057–2116. https://doi.org/10.5194/gmd-10-2057-2017

Murray, L. T., Logan, J. A., & Jacob, D. J. (2013). Interannual variability in tropical tropospheric ozone and OH: The role of lightning. *Journal of Geophysical Research*, *118*, 1–11. https://doi.org/10.1002/jgrd.50857

Murray, L. T., Mickley, L. J., Kaplan, J. O., Sofen, E. D., Pfeiffer, M., & Alexander, B. (2014). Factors controlling variability in the oxidative capacity of the troposphere since the Last Glacial Maximum. *Atmospheric Chemistry and Physics*, *14*, 3589–3622. https://doi.org/10.5194/acp-14-3589-2014

Naik, V., Horowitz, L. W., Fiore, A. M., Ginoux, P., Mao, J., Aghedo, A. M., & Levy, H. (2013). Impact of preindustrial to present-day changes in short-lived pollutant emissions on atmospheric composition and climate forcing. *Journal of Geophysical Research: Atmospheres*, *118*, 8086–8110. https://doi.org/10.1002/jgrd.50608

Naik, V., Voulgarakis, A., Fiore, A. M., Horowitz, L. W., Lamarque, J.-F., Lin, M., et al. (2013). Preindustrial to present-day changes in tropospheric hydroxyl radical and methane lifetime from the Atmospheric Chemistry and Climate Model Intercomparison Project (ACCMIP). *Atmospheric Chemistry and Physics*, *13*, 5277–5298. https://doi.org/10.5194/acp-13-5277-2013

Nicely, J. M., Duncan, B. N., Hanisco, T. F., Wolfe, G. M., Salawitch, R. J., Deushi, M., et al. (2020). A machine learning examination of hydroxyl radical differences among model simulations for CCMI-1. *Atmospheric Chemistry and Physics*, *20*, 1341–1361. https://doi.org/10.5194/acp-20-1341-2020

Orbe, C., Plummer, D. A., Waugh, D. W., Yang, H., Jöckel, P., Kinnison, D. E., et al. (2020). Description and evaluation of the specified-dynamics experiment in the chemistry-climate model initiative. *Atmospheric Chemistry and Physics*, *20*, 3809–3840. https://doi.org/10.5194/acp-20-3809-2020

Patra, P. K., Saeki, T., Dlugokencky, E. J., Ishijima, K., Umezawa, T., Ito, A., et al. (2016), Regional methane emission estimation based on observed atmospheric concentrations (2002–2012), *Journal of the Meteorological Society of Japan*, *94*(1), 91–113. https://doi.org/10.2151/jmsj.2016-006

Rice, A. L., Butenhoff, C. L., Teama, D. G., Röger, F. H., Khalil, M. A. K., & Rasmussen, R. A. (2016). Atmospheric methane isotopic record favors fossil sources flat in 1980s and 1990s with recent increase. *Proceedings of the National Academy of Sciences of the United States of America*, *113*, 10791–10796. https://doi.org/10.1073/pnas.1522923113

Saunois, M., Stavert, A. R., Poulter, B., Bousquet, P., Canadell, J. G., Jackson, R. B., et al. (2020). The global methane budget 2000–2017. *Earth System Science Data*, *12*, 1561–1623. https://doi.org/10.5194/essd-12-1561-2020

Schaefer, H., Fletcher, S. E. M., Veidt, C., Lassey, K. R., Brailsford, G. W., Bromley, T. M., et al. (2016). A 21st century shift from fossil-fuel to biogenic methane emissions indicated by $^{13}CH_4$. *Science*, *352*(6281), 80–84. https://doi.org/10.1126/science.aad2705

Spivakovsky, C. M., Logan, J. A., Montzka, S. A., Balkanski, Y. J., Foreman-Fowler, M., Jones, D. B. A., et al. (2000). Three-dimensional climatological distribution of tropospheric OH: Update and evaluation. *Journal of Geophysical Research*, *105*(D7), 8931–8980. https://doi.org/10.1029/1999JD901006

Stevenson, D. S., Zhao, A., Naik, V., O'Connor, F. M., Tilmes, S., Zeng, G., et al. (2020). Trends in global tropospheric hydroxyl radical and methane lifetime since 1850 from AerChemMIP. *Atmospheric Chemistry and Physics*, *20*, 12905–12920. https://doi.org/10.5194/acp-20-12905-2020

Taylor, K. E., Williamson, D., & Zwiers, F. (2000). *The sea surface temperature and sea-ice concentration boundary conditions of AMIP II simulations (Report 60 UCRL-JC-125597)*. Program for Climate Model Diagnosis and Intercomparison, Lawrence Livermore National Laboratory, University of California. https://pcmdi.llnl.gov/report/pdf/60.pdf?id=22

Tsuruta, A., Aalto, T., Backman, L., Hakkarainen, J., van der Laan-Luijkx, I. T., Krol, M. C., et al. (2017). Global methane emission estimates for 2000–2012 from Carbon Tracker Europe-CH_4 v1.0. *Geoscientific Model Development*, *10*, 1261–1289. https://doi.org/10.5194/gmd-10-1261-2017

Turner, A. J., Frankenberg, C., Wennberg, P. O., & Jacob, D. J. (2017). Ambiguity in the causes for decadal trends in atmospheric methane and hydroxyl. *Proceedings of the National Academy of Sciences of the United States of America*, *114*, 5367–5372. https://doi.org/10.1073/pnas.1616020114

van Marle, M. J. E., Kloster, S., Magi, B. I., Marlon, J. R., Daniau, A.-L., Field, R. D., et al. (2017). Historic global biomass burning emissions for CMIP6 (BB4CMIP) based on merging satellite observations with proxies and fire models (1750–2015). *Geoscientific Model Development*, *10*, 3329–3357. https://doi.org/10.5194/gmd-10-3329-2017

Voulgarakis, A., Naik, V., Lamarque, J. F., Shindell, D. T., Young, P. J., Prather, M. J., et al. (2013). Analysis of present day and future OH and methane lifetime in the ACCMIP simulations. *Atmospheric Chemistry and Physics*, *13*, 2563–2587. https://doi.org/10.5194/acp-13-2563-2013

Wild, O., Voulgarakis, A., O'Connor, F., Lamarque, J.-F., Ryan, E. M., & Lee, L. (2020). Global sensitivity analysis of chemistry-climate model budgets of tropospheric ozone and OH: Exploring model diversity. *Atmospheric Chemistry and Physics*, *20*, 4047–4058. https://doi.org/10.5194/acp-20-4047-2020

Zhao, M., Golaz, J.-C., Held, I. M., Guo, H., Balaji, V., Renson, R., et al. (2018a). The GFDL global atmosphere and land model AM4.0/LM4.0: 1. Simulation characteristics with prescribed SSTs. *Journal of Advances in Modeling Earth Systems*, *10*, 691–734. https://doi.org/10.1002/2017MS001208

Zhao, M., Golaz, J.-C., Held, I. M., Guo, H., Balaji, V., Renson, R., et al. (2018b). The GFDL global atmosphere and land model AM4.0/LM4.0: 2. Model description, sensitivity studies, and tuning strategies. *Journal of Advances in Modeling Earth Systems*, *10*, 735–769. https://doi.org/10.1002/2017MS001209

Zhao, Y., Saunois, M., Bousquet, P., Lin, X., Berchet, A., Hegglin, M. I., et al. (2019). Inter-model comparison of global hydroxyl radical (OH) distributions and their impact on atmospheric methane over the 2000–2016 period. *Atmospheric Chemistry and Physics*, *19*, 13701–13723. https://doi.org/10.5194/acp-19-13701-2019

Zhao, Y., Saunois, M., Bousquet, P., Lin, X., Berchet, A., Hegglin, M. I., et al. (2020). Influences of hydroxyl radicals (OH) on top-down estimates of the global and regional methane budgets. *Atmospheric Chemistry and Physics*, *20*, 9525–9546. https://doi.org/10.5194/acp-20-9525-2020

References From the Supporting Information

Evans, S., Ginoux, P., Malyshev, S., & Shevliakova, E. (2016). Climate-vegetation interaction and amplification of Australian dust variability. *Geophysical Research Letters*, *43*(11), 11823–11830. https://doi.org/10.1002/2016GL071016

Guenther, A. B., Jiang, X., Heald, C. L., Sakulyanontvittaya, T., Duhl, T., Emmons, L. K., & Wang, X. (2012). The model of emissions of gases and aerosols from nature version 2.1 (MEGAN2. 1): An extended and updated framework for modeling biogenic emissions. *Geoscientific Model Development*, *5*(6), 1471–1492. https://doi.org/10.5194/gmd-5-1471-2012

Horowitz, L. W., Walters, S., Mauzerall, D. L., Emmons, L. K., Rasch, P. J., Granier, C., et al. (2003). A global simulation of tropospheric ozone and related tracers: Description and evaluation of MOZART, version 2. *Journal of Geophysical Research*, *108*(24), 4784. https://doi.org/10.1029/2002JD002853

Jaeglé, L., Quinn, P. K., Bates, T. S., Alexander, B., & Lin, J. T. (2011). Global distribution of sea salt aerosols: New constraints from in situ and remote sensing observations. *Atmospheric Chemistry and Physics*, *11*(7), 3137–3157. https://doi.org/10.5194/acp-11-3137-2011

Lana, A., Bell, T. G., Simó, R., Vallina, S. M., Ballabrera-Poy, J., Kettle, A. J., et al. (2011). An updated climatology of surface dimethlysulfide concentrations and emission fluxes in the global ocean. *Global Biogeochemical Cycles*, *25*, GB1004. https://doi.org/10.1029/2010GB003850

Monahan, E. C., Spiel, D. E., & Davidsona, K. L. (1986). A model of marine aerosol generation via whitecaps and wave disruption. In E. C. Monahan, & G. M. Niocaill (Eds.), *Oceanic whitecaps* (pp. 167–174). Springer. https://doi.org/10.1007/978-94-009-4668-2_16